Journal of Structural Geology 32 (2010) 1070–1084

Contents lists available at ScienceDirect

Journal of Structural Geology

journal homepage: www.elsevier.com/locate/jsg

Stylolite interfaces and surrounding matrix material: Nature and role of heterogeneities in roughness and microstructural development

Marcus Ebner [a,*], Sandra Piazolo [b], Francois Renard [c,d], Daniel Koehn [a]

[a] Tectonophysics, Institute of Geosciences, Johannes Gutenberg University, Becherweg 21, D-55128 Mainz, Germany
[b] Department of Geology and Geochemistry, Stockholm University, 10691 Stockholm, Sweden
[c] University Joseph Fourier – Grenoble I/CNRS/LGCA/OSUG, BP 53, F-38041 Grenoble, France
[d] Physics of Geological Processes, University of Oslo, Norway

ARTICLE INFO

Article history:
Received 4 November 2009
Received in revised form
20 May 2010
Accepted 22 June 2010
Available online 30 June 2010

Keywords:
Stylolite
Pressure solution
Heterogeneities
Roughness
EBSD

ABSTRACT

Rough pressure solution interfaces, like stylolites, are one of the most evident features of localized slow deformation in rocks of the upper crust. There is a general consensus that the development of these rough structures is a result of localized, stress enhanced, dissolution of material along a fluid filled interface, but little is known on the initiation of this roughness. The aim of this article is to reveal the role of heterogeneities initially present in the host-rock on roughness initiation. This should give insights on whether stylolite roughness is generated by a stress-induced instability or by the presence of disorder in the material (i.e. quenched noise). We use a microstructural approach based on SEM/EBSD analysis combined with orientation contrast (OC) image analysis of stylolites in limestones. We found that the stylolite roughness is induced by heterogeneities in the host rock (clay particles and detrital quartz grains in our case). In addition, close to mature stylolite interfaces matrix modifications occur, which can be attributed to the compaction along the stylolite. The grain size decreases by 15–25% and a pre-existing shape- and lattice-preferred orientation (SPO, LPO) are significantly modified in the vicinity of the stylolite. The results presented here imply that localized pressure solution along stylolites is not necessarily restricted to the actual interface but influences the adjacent matrix. The heterogeneity data might serve as a quantitative basis for elaborate numerical models of localized compaction.

1. Introduction

Stylolites are localized pressure solution patterns characterised by a multi-scale roughness that spans several orders of magnitude ranging from serrated grain contacts at the micron-scale up to decimetre-scale roughness amplitudes. The intriguing morphological characteristics of pressure solution surfaces have been the main focus of many qualitative studies (Alvarez et al., 1978; Bathurst, 1987; Bayly, 1986; Buxton and Sibley, 1981; Dunnington, 1954; Guzzetta, 1984; Heald, 1955; Park and Schot, 1968; Stockdale, 1922), which in turn lead to more quantitative approaches (Andrews and Railsback, 1997; Railsback, 1993). In the last decade many studies employed statistical tools and characterised the stylolite roughness by its fractal geometry showing that stylolites exhibit a fractal scaling over several orders of magnitude (Drummond and Sexton, 1998; Karcz and Scholz, 2003). Some investigations of the 3D morphology of natural stylolites in limestones (Brouste et al., 2007; Ebner et al., 2009b; Renard et al., 2004; Schmittbuhl et al., 2004), in experimentally generated microstylolites (Gratier et al., 2005) and numerical simulations (Ebner et al., 2009a; Koehn et al., 2007) demonstrated that the stylolite roughness has two self-affine scaling invariances, which are separated at a characteristic crossover-length of a millimetre scale. These scaling regimes have distinct Hurst or roughness exponents of 1.1 and 0.5 for small and large scales, respectively. Quasi-universal scaling exponents were reported for bedding parallel stylolites from various different locations and with various lithological compositions (Brouste et al., 2007; Ebner et al., 2009b; Renard et al., 2004; Schmittbuhl et al., 2004).

Railsback (1993) and Andrews and Railsback (1997) showed that the morphological appearance and/or abundance of stylolites in carbonate rocks changes with the rock-type of the host rock. In addition the spatial density and intensity of dissolution seams were reported to correlate with the clay content in limestones and marls (Alvarez et al., 1978; Marshak and Engelder, 1985). Nevertheless the

* Corresponding author. Current address: Geological Survey of Austria, Neulinggasse 38, A 1030 Vienna, Austria. Tel.: +43 1 712 56 74 414; fax: +43 1 712 56 74 56.
E-mail address: marcus.ebner@geologie.ac.at (M. Ebner).

0191-8141/$ – see front matter © 2010 Elsevier Ltd. All rights reserved.
doi:10.1016/j.jsg.2010.06.014

cause for the roughness formation of both bedding parallel and tectonic (i.e. bedding perpendicular) stylolites remains unclear.

Based on field observations, microstructural investigations, numerical and analytical considerations two main concepts for the roughening of stylolites prevail. In the first (termed the *instability concept* here), a stress-induced roughening instability develops along an initially flat solid–solid interface (Angheluta et al., 2008) or solid–fluid–solid interface (Bonnetier et al., 2009). In the second (Ebner et al., 2009a; Koehn et al., 2007; Renard et al., 2004; Schmittbuhl et al., 2004), heterogeneities act as quenched noise and are responsible for the roughening of the interface (and therefore termed the *heterogeneity concept* thereafter). In contrast to the instability concept, the heterogeneity concept produces a rough surface but no instability as such. The heterogeneity in the system may be present as "pinning" particles that dissolve slower (Koehn et al., 2007) and "pin" the interface, which results in a roughness. Surface energy counteracts the effects of these pinning particles as a stabilizing term keeping the stylolite flat on small length-scales. In contrast to the instability concept, the stress is a stabilizing term (Schmittbuhl et al., 2004) in the heterogeneity concept and flattens the interface on large length-scales. It is therefore important to note that both concepts differ fundamentally, since in the instability concept the applied external stress causes the roughening and produces an instability, whereas in the second concept the heterogeneities in the material represent the key ingredient for roughening, and the stress drives the dissolution but produces no instability.

Models using heterogeneities as roughness origin have successfully generated synthetic surfaces in numerical simulations and analytical considerations that resemble the scaling features of natural stylolites (Brouste et al., 2007; Ebner et al., 2009a; Gratier et al., 2005; Koehn et al., 2007; Renard et al., 2004; Schmittbuhl et al., 2004). Although the importance of material disorder and composition on the stylolite morphology has been stressed in previous contributions investigating the rock hosting the stylolite (Andrews and Railsback, 1997; Railsback, 1993), so far no study quantitatively characterised the composition of the quenched disorder that initiates the distinct roughness of stylolite interfaces. This is indeed a difficult task in the field (Fig. 1) since pinning particles only rarely consist of macroscopically distinguishable rock-fragments (Fig. 1b) or bioclasts, and thus do not register in the macroscopic roughness scaling. In previous microstructural studies, the matrix around stylolites was mainly investigated in terms of porosity reduction and its influences on fluid flow in sandstones (Baron and Parnell, 2007; Harris, 2006; Mørk and Moen, 2007) and limestones (Carrio-Schaffhauser et al., 1990; Raynaud and Carrio-Schaffhauser, 1992). There is a general agreement among previous workers that pressure solution along stylolites provides a local source for cement around them. Low porosity haloes of up to several cm in width are reported (Baron and Parnell, 2007; Harris, 2006), but close examination under the SEM demonstrated that the porosity in the vicinity of the stylolite increases (within a few microns). This was termed the 'process zone' by Carrio-Schaffhauser et al. (1990), which is surrounded by a low porosity zone.

Microstructural investigations of experimentally compacted sandstones (van Noort et al., 2008) and drilled sandstone samples from the North Sea (Mørk and Moen, 2007), demonstrated that plastic deformation occurs around intergranular and localized pressure solution features. These authors report the occurrence of micro-cracks and Dauphiné twins from grain–grain contacts and show that Dauphiné twins are localized around stylolites. This demonstrates that localized pressure solution features concentrate stresses. Therefore they have to be carefully investigated to understand the dynamic evolution of stylolite formation from an initial interface with an undisturbed matrix to a mature interface with a modified host-rock matrix, which will in turn modify the pressure solution process as such.

Based on SEM and EBSD investigations we report direct evidence that multi-scale heterogeneities in limestones are an agent for the formation of stylolite roughness. In addition we describe matrix microstructures around mature stylolite interfaces and discuss their significance for localized pressure solution.

2. Dataset and methods

2.1. Stylolite dataset

We report the microstructural analyzes of four limestone samples from three different locations and geological settings (mid-Cretaceous limestones of south-eastern France *Nan1*, upper Jurassic limestones from southern France *N2* & *N7*, and southern Germany *Sa7b;*). The oriented samples were selected to cover the following range of stylolite characteristics: (i) initial to mature interfaces (for definition see below); (ii) different rock-texture hosting the stylolites e.g. mudstone to packstone and (iii) bedding parallel and tectonic stylolites.

The first locality, Cirque de Navacelles (Larzac), is located 50 km NW of Montpellier in southern France (*UTM 31T E 0539704 m; N 4860040 m*), exposing a flat-lying upper Jurassic limestone succession (Bodou, 1976; Rispoli, 1981). The outcrop is part of an external shelf deposit of the Vocontian Basin and consists mainly of fine-grained mudstones and wackestones. The top part of the succession is made of massive Kimmeridgian limestones, whereas the lower part exposes well-bedded Oxfordian slightly dolomitized mudstones (Bodou, 1976). Sub-horizontal bedding parallel and vertical tectonic stylolites can be found in the area. The horizontal set formed during burial, whereas the second vertical set formed due to Eocene N–S directed compression during the Pyrenean orogeny (Ebner et al., 2009b; Petit and Mattauer, 1995; Rispoli, 1981). We use only bedding parallel stylolites from this locality for our study. The lithology of the two investigated samples (*N2* & N7) are well-bedded Oxfordian mudstone.

The second investigated locality is sited 10 km south of Tübingen (Swabian Alb, southern Germany) and comprises upper Jurassic (Oxfordian to Kimmeridgian) limestones (Geyer and Gwinner, 1991). The Swabian Alb of southern Germany forms a region of flat-lying mainly marine Jurassic deposits. The investigated outcrop (*UTM 32U; E 0*521508 *m; N* 5370938 *m*) is made of bedded Oxfordian limestones (Etzold et al., 1996; Geyer and Gwinner, 1991), with bedding, slightly dipping ($<5^{\circ}$) towards the SE. The investigated sample (*Sa7b/1*) exhibits a vertical set of tectonic stylolites, trending WNW–ESE and recording an NNE–SSW compression. This NNE–SSW directed shortening is related to late Cretaceous compression in central Europe (Geyer and Gwinner, 1991; Kley and Voigt, 2008). The stylolite itself is hosted in a fine-grained calcite mudstone.

The third locality, Gorge du Nan, is situated 20 km East of Grenoble (SE France) in the Vercors Plateau. The outcrop (*UTM 31T E 0690591 m; N 5004233 m*) is located in the Urgonian carbonate platform (Moss and Tucker, 1995) of mid-Cretaceous age (Arnaud-Vanneau and Arnaud, 1990). The stratigraphy of the Urgonian platform consists of a Barremian bioclastic limestone Formation (Borne and Glandasse Formations) in the lower part and in the upper part of an upper Barremian to mid-Aptian Urgonian Limestone Formation (Arnaud-Vanneau and Arnaud, 1990; Moss and Tucker, 1995). The sample (*Nan1*) investigated in this study belongs to the lower Orbitolina Beds (Apt) and is a packstone–grainstone with grains consisting of foraminifera and ooids. The investigated stylolites are bedding parallel that presumably formed during burial.

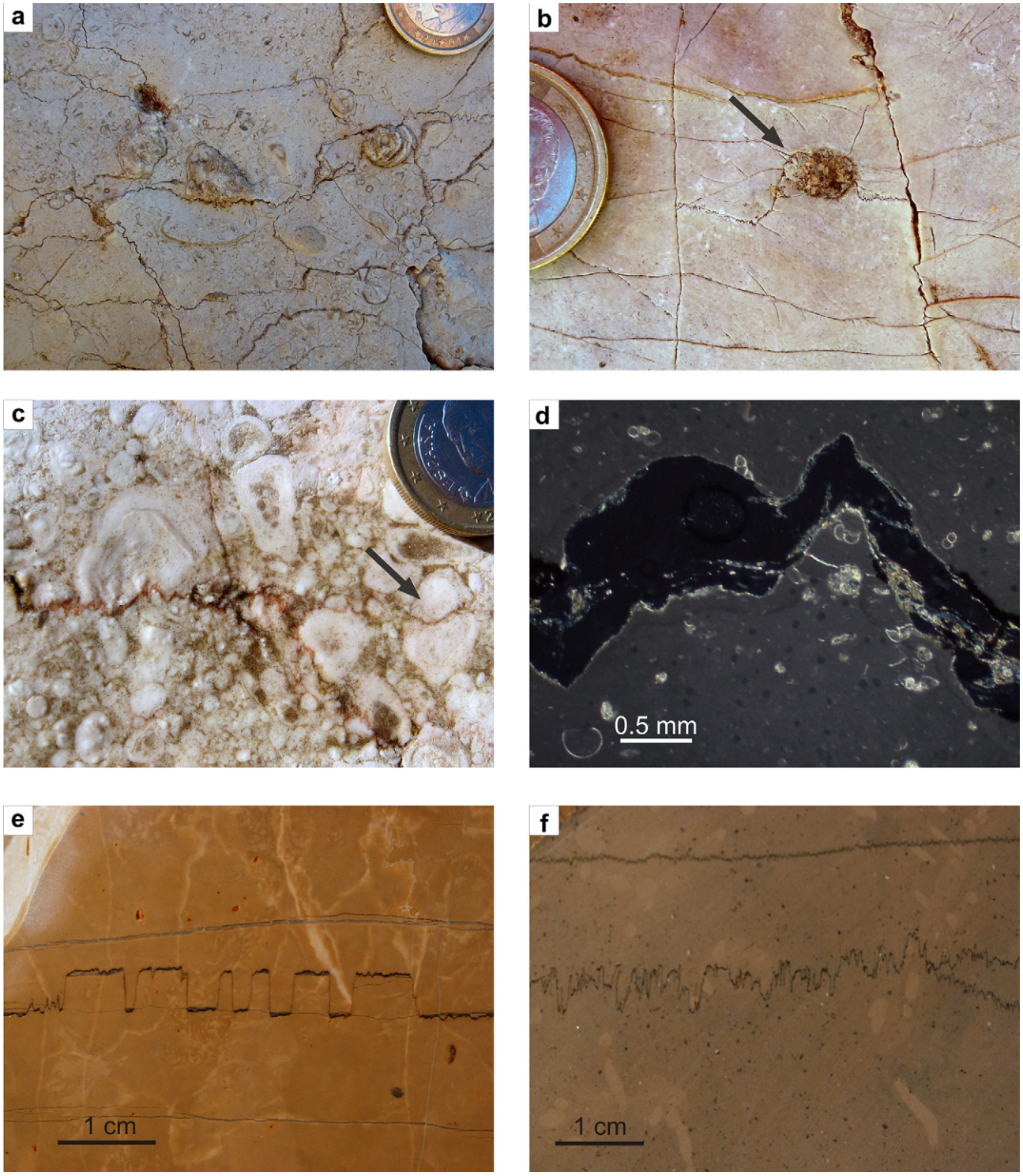

Fig. 1. Photographs of stylolites in limestones and their relationship to a macro and microscopic pinning components. a)–d) Biogenic clasts, i.e. mollusca, foraminiferea, which do not register in roughness. Particles which do register in the roughness are indicated with an arrow. e) Stylolite whose development was inhibited by a horizontal calcite vein and thus forms a columnar morphology. f) Small clay aggregates in the matrix around a stylolite. Note that macroscopic clay particles are larger than the smallest amplitudes of the stylolite. One euro coin for scale. Images in a & c from outcrops located in the Iberian Chain (NE Spain) (Ebner et al., 2010), b & d form Gorge du Nan (SE France), e from the Swabian Alb (SW Germany) and f from Cirque the Navacelles (S France). Compare text for details.

2.2. Methodology (EBSD and OC settings)

All samples were investigated using optical and scanning electron microscopy (SEM) with electron backscatter diffraction (EBSD) coupled with forescatter orientation contrast (OC) imaging. Forescatter detectors provide orientation contrast and phase (atomic number, z) contrast of samples (Prior et al., 1999, 1996). The analysis was performed on polished thin-sections that remained uncoated. To reduce charging of conductive material, the analyzes were conducted at low vacuum and the thin-sections

were fixed to a holder with conductive double sided adhesive carbon tape. The EBSD and OC data were collected at Stockholm University with a *Phillips XL-30 FEG-ESEM* in combination with a *Nordlys* detector and the *Oxford Instruments HKL Channel5* acquisition software (Flamenco). The samples were oriented with a high tilt angle of 70° and the SEM was operating at 20 kV and a 10 nA current at a working distance of 20 mm. To analyze the resulting electron back scatter pattern (EBSP) we set the indexing limit to a band detection of 6 (min)–7 (max) of 72 [hkl] theoretical reflectors. The acquisition speed was between 0.1 and 0.03 s/measurement point (sample *N2 & N7* 0.095s/pt; *Nan1* 0.0047s/pt & *Sa7b* 0.003s/pt). The EBSD maps were constructed from a step size of 0.2 μm (*N7*) and 0.4 μm (*N2, Nan1, Sa7b*) and usually contain a minimum of several hundred up to 70,000 grains. The average indexing was around 50–70% (if holes and grain boundaries are considered, indexing was above 80%). Using the *HKL Channel5* analysis software we interpolated the raw data by replacing non-indexed pixels with more than five neighbours with an orientation of the neighbouring pixels. In addition we filtered isolated pixels with a 60° misorientation with respect to its neighbours and replaced them with an orientation of the neighbouring pixels. We define grains such that a lattice misorientation of EBSD measurement points between 2° and 10° is a subgrain boundary and a misorientation >10° a high angle grain boundary. Measurement points that are not separated by a boundary are clustered into grains. We then analyze the grain size and shape.

To quantify the grain size, shape and distribution of clay particles in the vicinity of stylolites we utilize a digital image processing tool *Analyze Particles* (Heilbronner and Keulen, 2006; Heilbronner, 1992; Panozzo, 1983) implemented into the public domain software *ImageJ*. For our analyzes we use OC images as in these images clay particles are bright white and easily separable from the medium grey-values of the calcite matrix (compare Fig. 2). By segmentation of the greyscale bitmap images, the (white) clay could be separated from the (grey) calcite and could consequently be analyzed quantitatively using the image analysis routine *Analyze Particles*.

3. Data analysis & results

In this section we first describe observations of heterogeneities along and around stylolites (Sections 3.1 and 3.2), which we attempt to corroborate by a more quantitative analysis of the matrix (including crystallographic orientation, grain size and shape analysis) and the identified quenched disorder (grain size and shape analysis). Then, in Section 3.3, we focus on matrix adjustments around a mature pressure solution interface of a tectonic stylolite.

3.1. Noise around initial interfaces

Initial interfaces, which are here defined as interfaces that have not developed a continuous residual layer, *i.e.* a through going clay parting, are considered crucial to the understanding of the origin of the roughness along stylolite interfaces. Fig. 2 shows a series of orientation contrast (OC) images of sample *Nan1,* which all contain an initial horizontally-oriented microstylolite, *i.e.* visible only under the microscope. In Fig. 2, the grey matrix is made up of calcite crystals, where individual grains can be distinguished by different greyscale levels reflecting a change of the lattice orientation between adjacent grains (Prior et al., 1996). In the following the term grain is used for a crystallographically distinguishable unit, without any genetic meaning. The same applies for the term matrix which is not used as a genetic term but for the groundmass of the rock forming mineral in the vicinity of the stylolite. The bright spots in the OC image are clay minerals of various sizes. Only a limited amount of charging (i.e. white halos around grains with a high relief) occurs along single grains. The microstylolite itself is

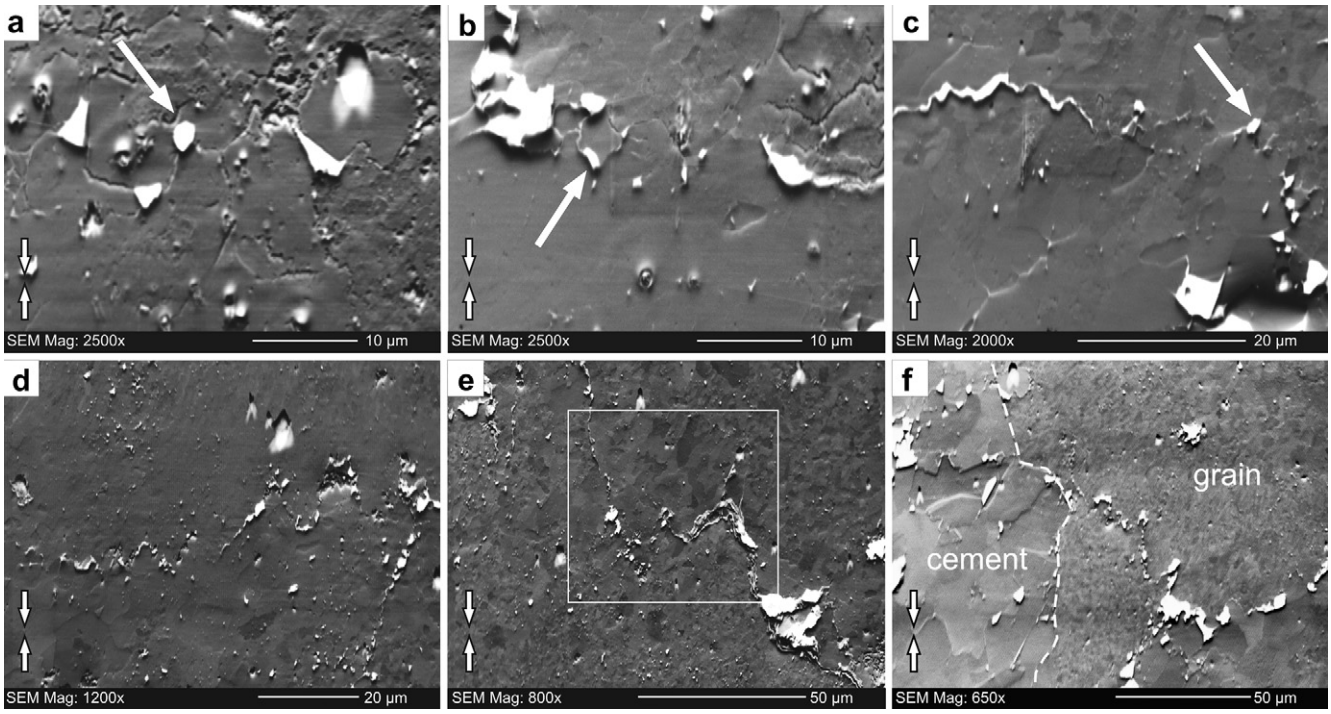

Fig. 2. Orientation contrast (OC) images of initial stylolites in fine-grained calcite limestones. All images are from sample Nan1. White spots are clay particles and the dark grain groundmass is calcite a)–c) Clay particles are located at the topmost part of the asperities along microstylolites (white arrow). d)–f) Microstylolites which have accumulated more residual clay and thus indicate higher strains. The white frame in e) indicates the area analyzed with EBSD shown in Fig. 4a. Small opposing arrows indicated stylolite compaction direction inferred from teeth orientation.

represented as a thin black line (Fig. 2a), i.e. a depression, which is not hit by the electron current due to the high sample tilt.

One important observation is the alignment of clay particles atop pronounced teeth, *i.e.* on the convex side along these microstylolites (indicated by white arrows in Fig. 2a–c). Although there is a roughness along Calcite–Calcite contacts (e.g. Fig. 2a), a significant amount of the prominent asperities along the interface are occupied with clay particles. Looking at slightly higher strains (Fig. 2d–f), increasingly more clay particles align along the stylolite interface. The amplitude of the roughness is larger than the grain size of the clay particles. Calcite grain size (see Fig. 2f) varies because sparitic cement fills the pore space of the grainstone and fine-grained biogenic calcite occurs in bioclasts and onkoids. Localized pressure solution can either occur along zones of grain size variation (Fig. 2d) or within zones of homogeneous grain size (Fig. 2e and 2f). In addition, we noticed that the grain size of the pinning particles, i.e. the clay particles, changes along individual microstylolites (Fig. 2f). In the regions of sparitic calcite (pore filling) cement the grain size of the clay minerals is usually larger than in the fine-grained bioclast material.

The results of the grain size and shape analysis of sample *Nan1* are shown in Fig. 3a and Table 1a. The figure shows the relative frequencies of grain surface area [μm^2] and circle equivalent diameter [μm], (the diameter of a circle that has the same surface area as a given grain). In the following we use the grain surface area as the characteristic quantity for the grain size. Comparison to other common measurements of the grain size (Humphreys, 2001), like the linear intercept method (not presented in this study), reveal the same results (compare Table 1a). Following Mingard et al. (2007), Fig. 3 is best represented by the geometric mean if the geometric mean equals (or is very close to) the natural logarithm of the median of the grain surface area. Since this is the case, we will use the geometric mean 1.0 μm^2 to represent the mean grain surface area.

To characterize the grain shape we utilize best-fit ellipses calculated for individual grains (Table 1a). We calculate the aspect ratio a/b with a and b being the major and minor axis of the best-fit ellipse and θ, the counter clockwise angle of the map base and the long ellipse axis a. For the grain shape analysis we only use grains with an area >1.5 μm^2. This procedure allows reducing artefacts introduced by the square pattern of the grid and the resolution limit of 0.4 μm. Otherwise the resulting histogram is strongly biased since bins in the region of 0°, 45°, 90° and 135° are overrepresented. This moderate shape preferred orientation with grains aligned in a direction 76° from the map base is not related to pressure solution but can be attributed to radial growth in spherolitic calcite particles (the investigated maps contain such calcite particles made of large crystals). The observed shape preferred orientation is not due to pressure solution since the shortening direction is normal to the base of the map so that preferential dissolution of grains along grain boundaries that are aligned perpendicular to the shortening direction should result in a clustering of the long axis of these grains parallel to the base (i.e. θ of 0° or 180°), a pattern that is not observed. Fig. 3b shows the same results for sample *N7* (also compare Table 1a).

The analysis of the lattice preferred orientation (LPO) of calcite around pressure solution surfaces is based on the EBSD measurements. The LPO data of the samples *Nan1* (Fig. 4a; corresponds to the area indicated by the white frame in Fig. 2e) and *N7* (Fig. 4b) are represented in equal area upper hemisphere pole figures of the *c* (0001), *r*(10–14), *a*(11–20) and *f*(01–12) poles. For sample *Nan1* and *N7*, is N–S and E–W in the analyzed area coordinate system, respectively. *Nan1* generally does not show a preferred LPO for any of the shown crystal planes (Fig. 4a). However, there are distinct maxima of the c-poles, which correspond to a preferred crystallographic orientation of large biogenic calcite crystals identified as such individually in the EBSD maps and under the SEM. The pole figures of sample *N7* show a near random LPO, with no distinct pattern related to the compaction direction.

In a third step, we quantitatively analyze the quenched noise, *i.e.* the heterogeneities initially present in the host-rock, which we have identified qualitatively (see above). Clay particles distributed in the host-rock are observed to be sites where asperities along the stylolite interface form primarily (Fig. 2). Resulting grain area, circle equivalent diameter, aspect ratio and θ are shown in Fig. 6 and Table 1b. The orientation of the clay particles (θ) in both samples is similar to the orientation of the calcite grains (see Fig. 3).

In addition we investigated the distribution of the clay particles following the approach of Heilbronner and Keulen (2006). The quenched noise density image (Fig. 5), which shows the density or distribution of the heterogeneities (clay particles in our case) in the image, is calculated after applying a Gaussian filter to the segmented black-and-white bitmap images (Fig. 5a) with a square kernel size of 25 pixels. The Gaussian filter ensures that the average density of the filtered image (Fig. 5b) is the same as that of the original bitmap (Fig. 5a). Fig. 5c shows the contours in % cross-sectional area of clay particles. For both samples (Nan1 & *N7*) no clear relationship between clay particle distribution and compaction direction or calcite orientation is observed. Such a lack of relationship indicates a quasi random clay particle distribution.

3.2. Noise around mature interfaces

Mature stylolite interfaces, which have accumulated a continuous residual clay layer, generally exhibit higher strains and rougher topography (Koehn et al., 2007). The investigated sample *Sa7b*, is a fine-grained Jurassic limestone, which contains such a mature tectonic (bedding normal) stylolite which reveals an NNE–SSW directed compression (Kley and Voigt, 2008). Fig. 7a shows an OC image of a characteristic segment of the stylolite interface. The dark grey groundmass is calcite and the bright white material is clay material/particles. Note that the accumulated residual clay layer has a thickness of up to 250 μm measured parallel to the compaction direction. It is interesting to notice that the top boundary of the residual clay layer is rather smooth with straight segments connected by narrow bends, whereas the lower boundary is jagged. This thickness variation cannot be explained by abrupt changes in abundance of clay content along the interface (compare Fig. 7a; examined below), *i.e.* we assume a rather constant distribution of clays at our scale of observation. In addition, a qualitative change in the distribution of the clay particles cannot be observed across the interface. We noticed that grains with a high relief, indicative of a different resistance to the polishing of the thin section, occur at these indentations (Fig. 7b; arrow). EBSD analysis of these areas reveals the presence of quartz grains at these indentation sites along the residual clay layers (Fig. 7c and d).

The quantitative investigation of the mature stylolitic interface follows the same procedure as in the previous section. Fig. 8 shows the quantitative data for the calcite grains (Fig. 8a), which is again based on the grain reconstruction from the EBSD measurements, and the clay particles (Fig. 8b) based on image analysis of OC images. (compare Tables 1a and b).

Although there is a striking similarity between the SPO of calcite and clay particles, it is important to note that clay particles are almost one order of magnitude smaller and have a higher aspect ratio than the calcite grains due to their platy morphology. We also analyzed the distribution of the clay particles (not shown) but did not observe a correlation with the thickness variation of the interface or compaction direction (see Fig. 5). The quartz grains

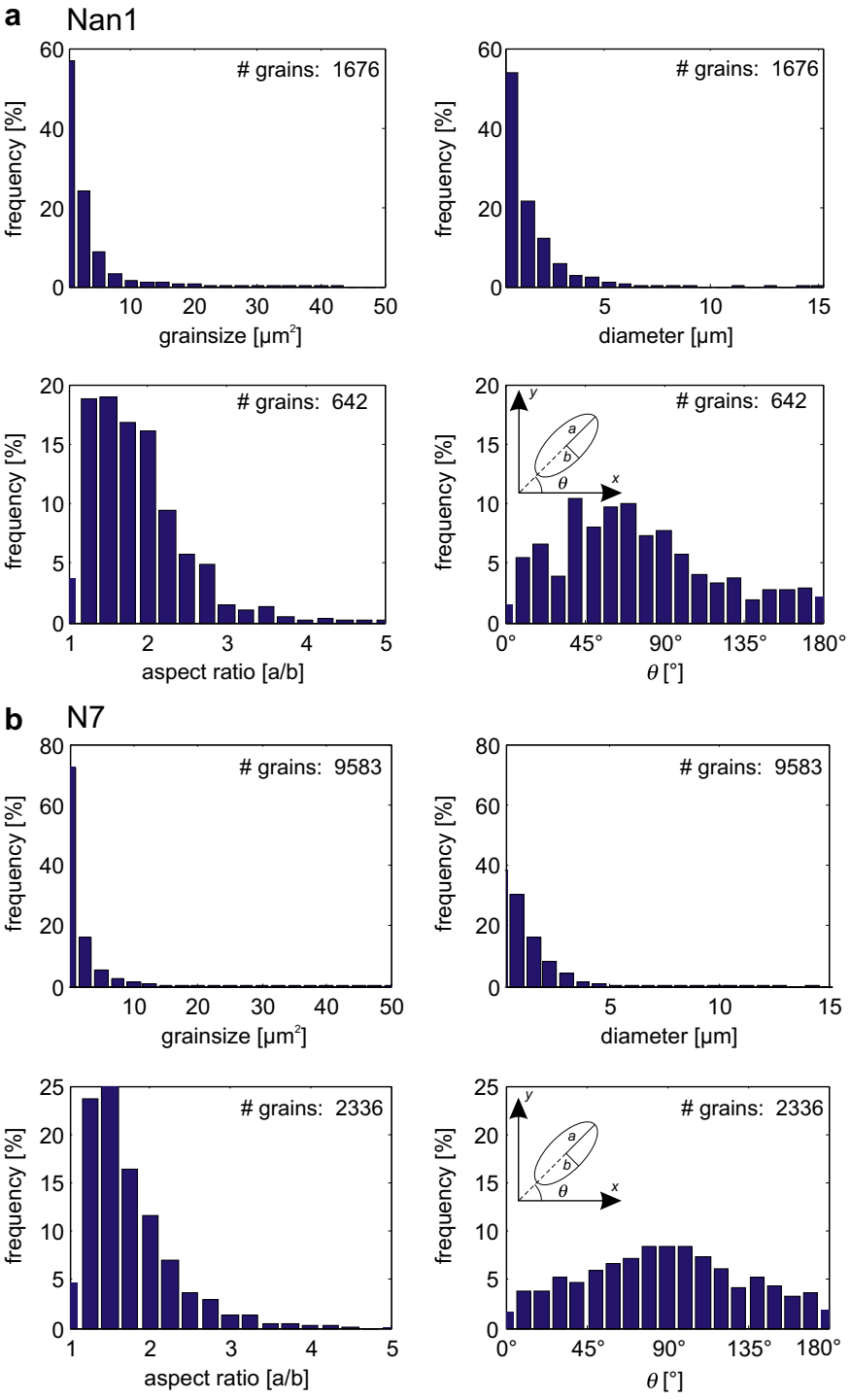

Fig. 3. Graphs showing relative frequencies of (cross-sectional) *grain surface area* (µm^2), *circle equivalent diameter* (µm), *aspect ratio* (*a*/*b*), θ (○) from individual calcite grains reconstructed from EBSD measurements (see Section 3.2). Small inset shows how *aspect ratio* and θ are calculated from best fitting ellipses of individual grains. Reference frame refers to the orientation of the EBSD map. Note that for *aspect ratio* and θ only grains ≥1.5 µm^2 a) Sample Nan1, (number of grains 1676) mean grain area 3.1 µm^2 b) Sample *N7*, (number of grains 9582) mean grain area 2.1 µm^2.

(identified by their EBSP) were digitized manually using *ImageJ* and the grain surface area was calculated following the method described above (See Table 1b).

3.3. Matrix adjustments around mature interfaces

To investigate the adjustments of the matrix around stylolite interfaces we examine a large map of Sample *Sa7b*. The selected map contains a stylolite peak with an amplitude of several hundred microns. Fig. 9a shows an OC image of the stylolite peak with a frame outlining the lower part of the EBSD map shown (Fig. 9b). The EBSD map with a size of 300 × 865 µm and a resolution of 0.4 µm contains some 1.6 million EBSD measurements. The inset in Fig. 9b shows the location of investigated subsets above the interface (relative to the base of the image) *a*–*j* and below the interface *-a* & *-b*. The subsets were chosen to be located parallel to the local

Table 1
Tabulated data and results of investigated samples. *a)* EBSD data from calcite and *b)* orientation contrast image analysis data from calcite and clay.

EBSD measurements (calcite)						
Sample	Spot size [μm]	# Analyzed grains/ map area [μm^2]	Grain area (arith. mean/ geom. mean/±std) [μm^2]	Circle equivalent diameter (mean/median) [μm]	Aspect ratio [a/b] of best fitting ellipse (mean/median)	Slope θ of long axis (mean/median) [°]
Nan1	0.4	1676/7967	3.1/1.0/±9.1	1.48/1.11	1.85/1.73	76/70
N7	0.2	9583/28462	2.0/0.35/±13.9	1.00/0.55	1.72/1.58	89/88
Sa7b	0.4	59450/258163	2.9/1.2/±5.1	1.58/1.28	1.65/1.54	76/71

OC image analysis (clay & quartz particles)							
Sample	Pixel size [μm]	# Analyzed grains/ image area [μm^2]	Surface fraction [%]	Grain area (arith. mean/ geom. mean/±std) [μm^2]	Circle equivalent diameter (mean/median) [μm]	Aspect ratio [a/b] of best fitting ellipse (mean/median)	Slope θ of long axis (mean/median) [°]
Nan1	0.12	876/25190	2.97	0.86/0.15/±3.17	0.66/0.42	2.14/1.92	76/67
N7	0.21	5171/96846	5.94	1.11/0.25/±5.51	0.80/0.50	1.91/1.72	89/90
Sa7b Clay	0.12	3650/34292	4.53	0.42/0.12/±1.26	0.54/0.38	2.04/1.83	78/73
Sa7b Quartz	0.84	38/559000	0.71	106.72/62.1/±131	10.31/8.90	1.70/1.62	82/91

topography of the interface to investigate possible effects of the distance to the interface on grain size, shape (SPO), lattice preferred orientations (LPO), and compression direction. Opposing arrows in Fig. 9b show the tectonic compression direction inferred from the stylolite teeth orientation, which is a reliable indicator of the compression direction (Koehn et al., 2007).

The grain size and shape analyzes were again based on EBSD measurements as outlined in Section 3.1, the complete dataset is shown in Fig. 8 and Table 1a and b Analyzing the individual subsets and plotting the grain surface area (Fig. 9c) and θ (Fig. 9d) as a function of the distance to the interface reveal considerable variations of these parameters.

Fig. 9c shows the arithmetic and geometric mean grain areas (μm^2) of individual subsets; the coefficient of variation being plotted as error-bars around the mean values. It is important to notice that the grain size remains constant in a range of 75–500 μm above the stylolite interface. Close to the stylolite, however, the grain size drops from an average of 1.2–0.9 μm^2 (geometric mean) in a region 25–75 μm from the interface and increases again to 1.2 μm^2 in a region <25 μm from the interface. Below the interface, the grain surface area is significantly larger, both arithmetic and geometric mean supporting this observation. The strong SPO (Fig. 9d; compare Fig. 8a for complete dataset) of the sample is also modified toward the interface. The average (arithmetic and geometric mean) and median angular values indicate a slight counter clockwise rotation of the SPO (5–10°) over a distance range of 100–500 μm, which is followed by a clockwise rotation of 5° in the next 75 μm. In the region adjacent to the interface (distance <25 μm) the SPO rotates 10° counter clockwise. Additionally the amount of asymmetry of the SPO, i.e. the kurtosis, generally decreases towards the interface.

The LPO of the investigated sample (Fig. 10) is given in the same representation as Fig. 4 (compare Section 3.1). The complete dataset shows a weak LPO with the *c* poles being oriented in a great

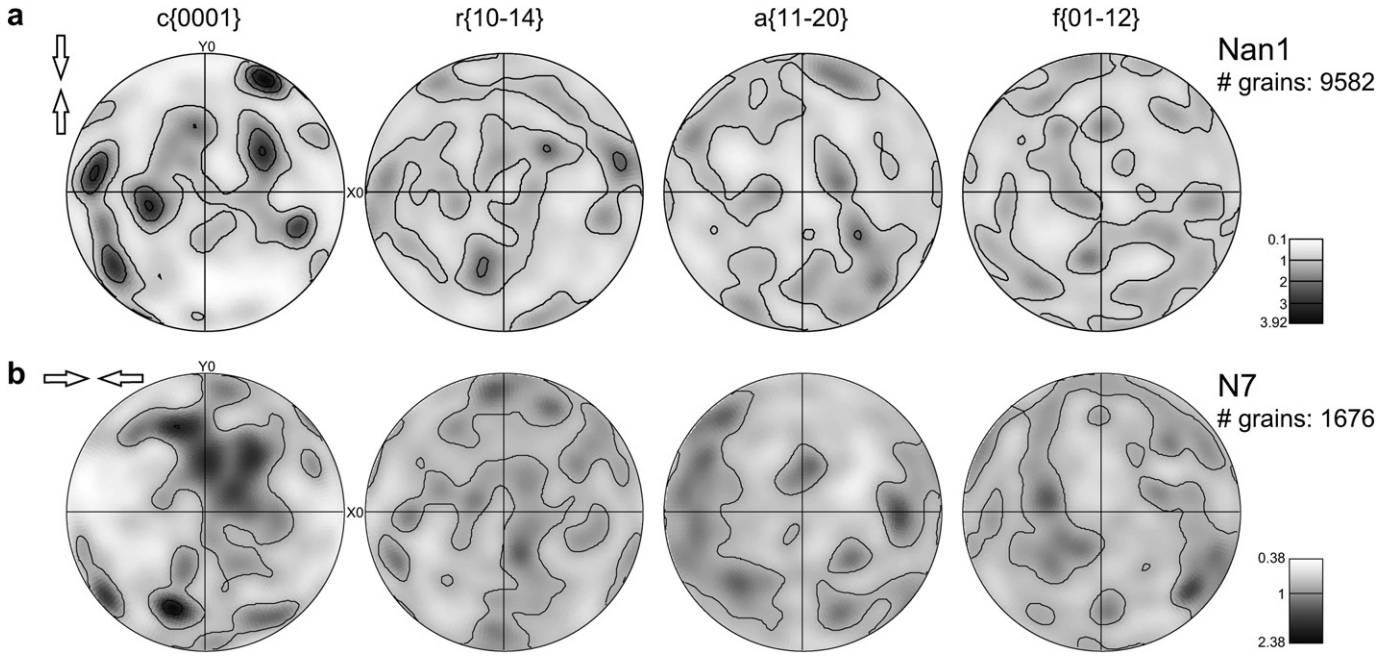

Fig. 4. Lattice preferred orientation (LPO) of calcite from EBSD analysis. Contoured pole figures of *c(0001)*-, *f(10–14)*-, *a(11–20)*- and *r(01–12)*-poles in equal area (upper hemisphere) projection. Contouring parameters: half width 15° and cluster size 5°. a) Sample Nan1 from Fig. 2e, (compaction direction N–S); b) Sample *N7* (compaction direction E–W). Both samples do not show an LPO which can be attributed to the compaction direction. Small opposing arrows indicated stylolite compaction direction inferred from teeth orientation.

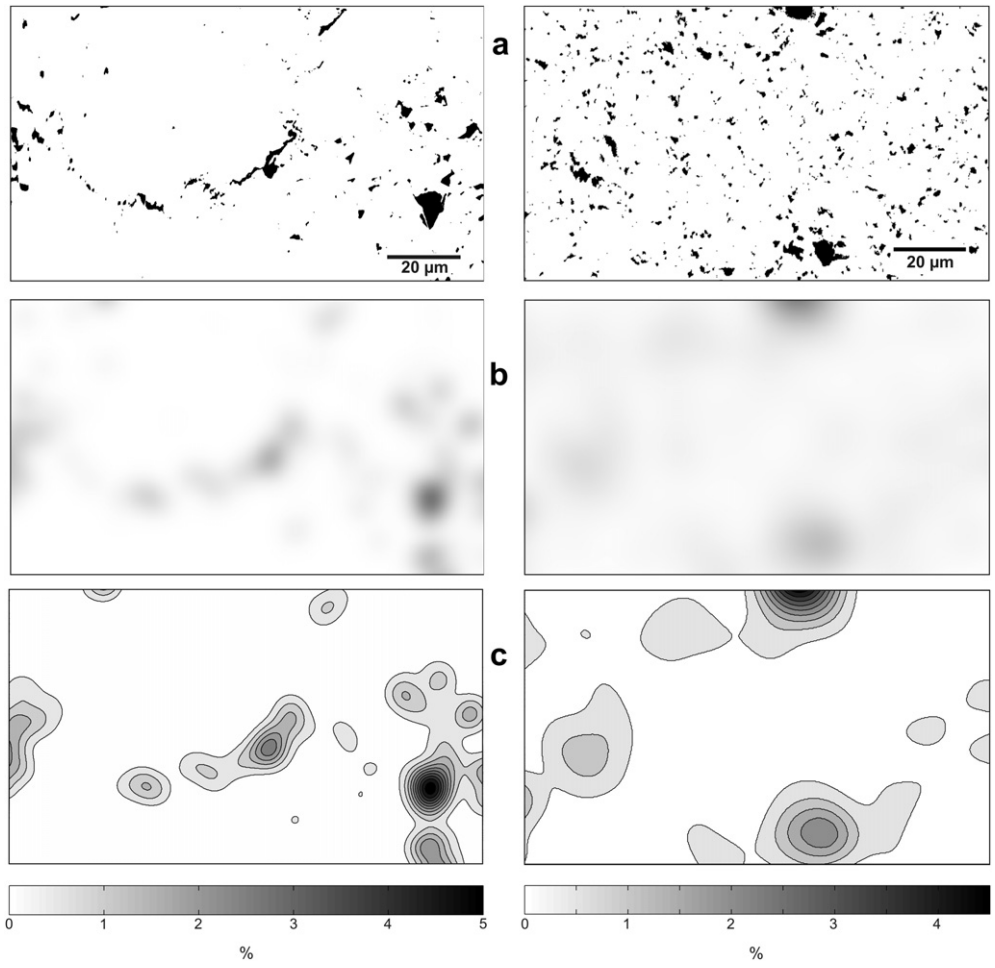

Fig. 5. Distribution analysis of clay particles in the host-rock surrounding the stylolite from samples Nan1 (left column) and *N7* (right column). a) Segmented clay particles (black dots) from OC images. b) Greyscale image with a Gaussian filter (kernel size 25 pixels) applied to the BW-bitmap in panel a to produce a density image. c) Density image contoured for % clay particles. No significant relationship between the distribution of the particles and the compaction direction can be seen. Compaction direction is N–S for *Nan1* (left column) and E–W for *N7* (right column).

circle roughly normal and the *a*-poles exhibit small circles oriented parallel to the sedimentary compaction direction. In the subsets e–j (defined in Fig. 9b) this orientation is more or less evident. In the vicinity of the stylolite interface (i.e. subsets a–d), the LPO is modified. The c-poles show a localized single maximum parallel to the tectonic shortening/compression direction and the a-poles show very weakly defined small circles normal to this shortening direction. The orientation of the *c*- and *a*-poles is similar to reported uniaxial compression experiments (Wenk, 1985; Wenk et al., 1987). Across the interface the LPO has a different orientation, with c-poles defining a great circle, which is aligned with neither the sedimentary compaction nor the tectonic compression direction. We do not observe an effect of twinning of calcite e.g. *e* or *r-twins*, in the sample, even though twinning is supposed to be the dominant low grade deformation mechanism in calcite polycrystals (Lacombe, 2007; Passchier and Trouw, 2005).

4. Discussion

We presented observations of heterogeneities initially present in the matrix surrounding both initial and mature stylolites. In addition we showed that a mature stylolite affects the adjacent matrix, though not limited to porosity occlusion. Thus, we will first discuss the heterogeneities and then focus on matrix adjustment and its significance for stylolite development and localized pressure solution in general.

4.1. Heterogeneities/quenched noise around stylolites

The work of Railsback (1993) and Andrews and Railsback (1997) demonstrated that stylolite morphology can be related to the host-rock lithology. They also argue that "lithologic heterogeneity" influences the morphology of stylolites e.g. more heterogeneous grainstones and packstones form more serrate morphologies than wackestones and mudstones. However, they did not characterise the heterogeneity that initiates the roughness of the stylolites beyond the Dunham classification. Based on thorough statistical analysis Brouste et al. (2007) showed that the scaling properties of stylolites change along the interface, which they argue is due to a variation of the heterogeneities (termed quenched disorder by them) in the material. Furthermore, analytical (Renard et al., 2004; Schmittbuhl et al., 2004) and numerical (Ebner et al., 2009a; Koehn et al., 2007) approaches have successfully used heterogeneities as a cause for the roughness. The results of the works cited above all indicate that heterogeneity plays an important role in the formation of stylolite roughness. Nevertheless none of the above studies directly proved the existence of heterogeneities nor did they show the composition or distribution of these heterogeneities.

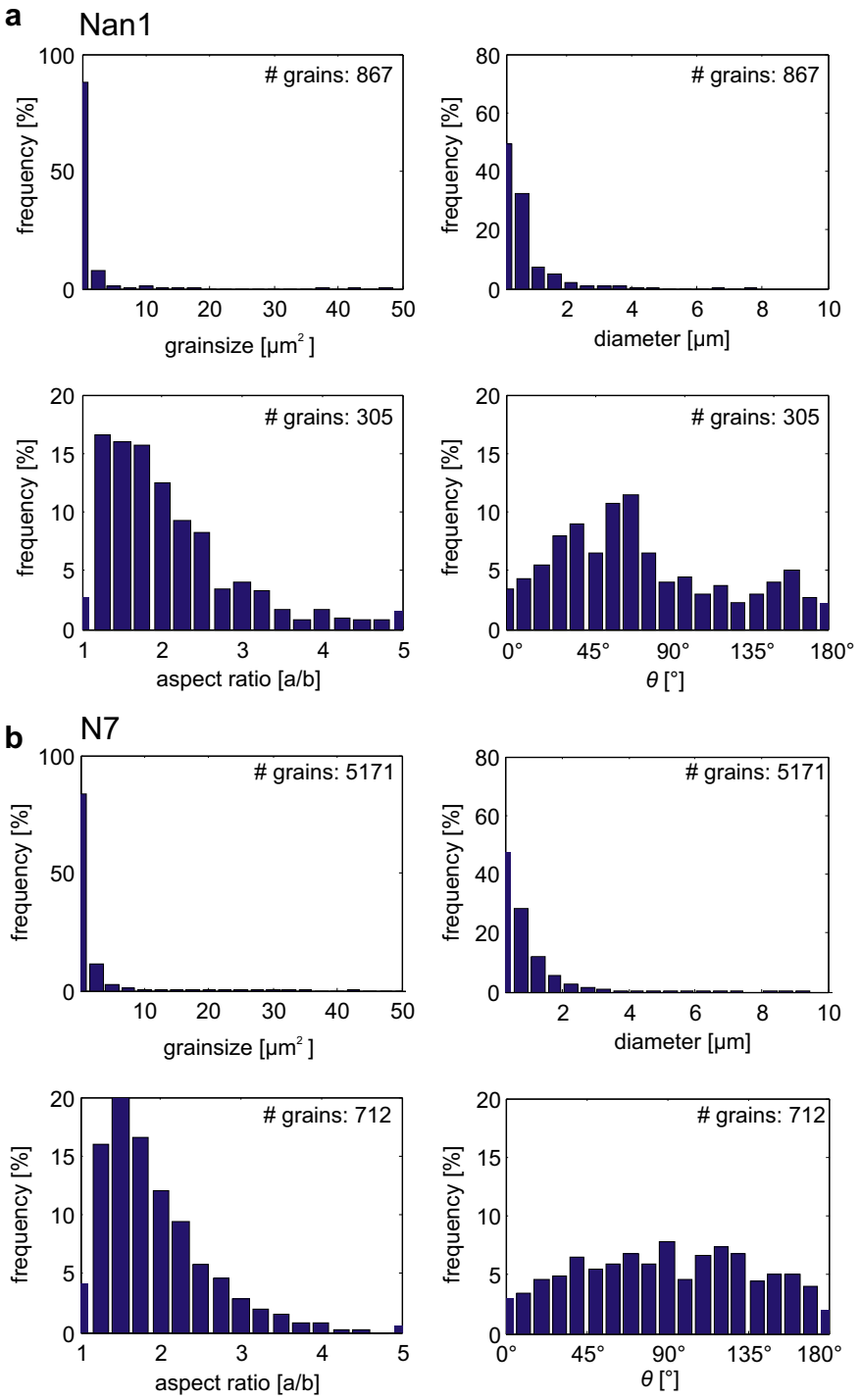

Fig. 6. Graphs showing relative frequencies of (cross-sectional) *grain surface area* (μm²), *circle equivalent diameter* (μm), *aspect ratio* (*a*/*b*), *θ* (○) of the individual clay particles analyzed with *ImageJ* similar to the data shown in Fig. 3. a) Nan1, 3.0% of clay material with an average grain surface area of 0.86 μm² (geometric mean 0.15 μm², pixel size 0.15 μm). b) *N7* contains 5.9% of clay material with an average grain surface area of 1.0 μm² (geometric mean 0.25 μm², pixel size 0.4 μm). Note that for the aspect ratio and *θ* only grains covering an area of more than 10 pixels are used.

In the present work we analyzed bedding parallel and tectonic stylolites hosted in limestones of varying Dunham classes and geological setting. We showed that heterogeneities, e.g. clay particles, play a crucial role in the formation of the distinctive roughness of stylolites. A considerable fraction of the larger stylolite peaks contain a clay particle on their convex side which implies that these heterogeneities act as pinning particles that tend to significantly change the relative dissolution rates on the respective side of the interface (Fig. 2). The fact that not all teeth are occupied by a clay particle can be explained (i) since not all 2D intersections of a 3D stylolite interface hit a clay particle or (ii) other heterogeneities play a role (see below). In general the clay particles are more than one order of magnitude smaller than the calcite grains. This rules out that stylolite roughness is a function of the host-rock grain size, which underlines the results of Karcz and Scholz (2003). Our observations also suggest that grain size variations are not a coercive prerequisite

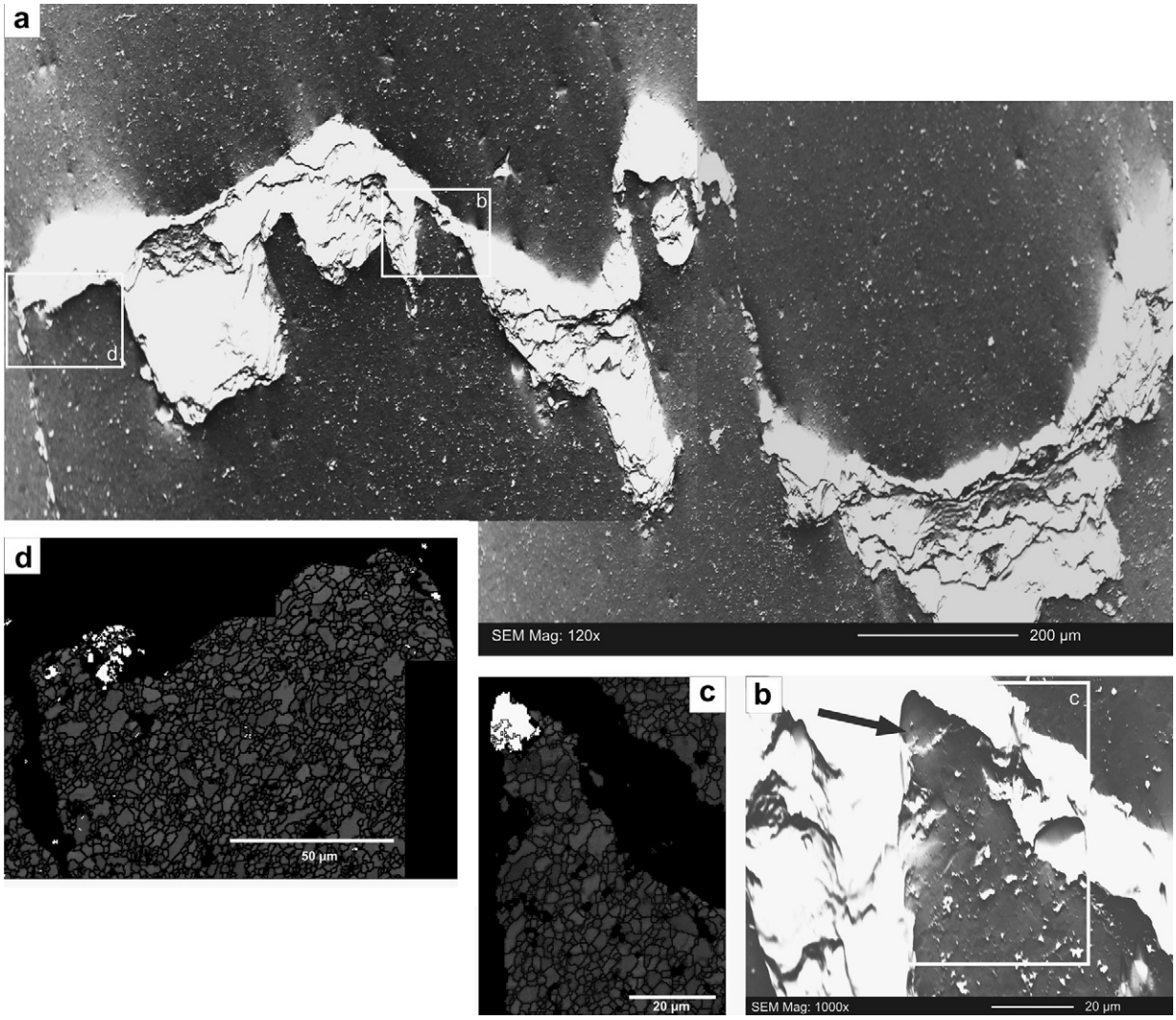

Fig. 7. OC images and EBSD maps of a mature tectonic stylolite (sample *Sa7b*). a) OC image showing a mature stylolite interface with significant thickness variation of the residual clay layer. Note that the topography changes from one side to the other. Frames indicated the enlargements in b & d. b) Enlargement of panel a showing the indentation in the residual clay layer. Arrow points to a grain with a high relief indicative for a different resistance to polishing. c) & d) EBSD maps of the enlarged areas in panels a) and b) showing the grain outline and a colour-coding for the material (grey – calcite; white – quartz). Quartz grains occupy all positions with a clear thickness variation of the residual clay layer.

for localization of pressure solution since we observe distinct pressure solution features in regions of either homogeneous or heterogeneous grain size. We also noticed that calcite–calcite contacts show irregular grain boundaries without any clay particles between them. This indicates that a different heterogeneity (e.g. chemical variations) possibly influences the roughening without the aid of clay particles. In addition we found detrital quartz grains along thickness variations in the residual clay layer of stylolite interfaces (Fig. 7). Since we could not attribute the thickness variation to a change in the distribution or abundance of the clay surrounding the interface, we argue that these quartz grains form a different class of pinning particles, which are resistant to dissolution. The quartz grains might also indent into the residual clay layer as soon as they hit the pressure solution surface and thus cause the columnar morphology seen in Fig. 7. Nevertheless we do not observe any convincing argument for brittle deformation around the quartz grains (e.g. radial fracturing emanating from the quartz grains).

The heterogeneities that we observe in this study (clay particles and quartz grains) cause the roughening of stylolites because they have a different resistance and/or kinetics of dissolution. The heterogeneities may span several orders of magnitude in size and vary in abundance and composition to form a multi-scale, polymict quenched noise. In our view, heterogeneities are not limited to the range of scales we have investigated (µm to dm); but probably exist on even smaller scales. For example, the rough calcite–calcite contacts imply that there is a different (smaller) heterogeneity, which might be a chemical variation, i.e. integration of Mg instead of Ca in the atomic lattice or a change in the elastic properties due to lattice defects. To resolve this issue, submicron scale chemical mapping and/or TEM analysis would be necessary. The pinning particles identified in this study might only be a small portion of the variety of heterogeneity that induces stylolite roughness. For example in stylolites in other lithologies, e.g. quartzite, other heterogeneities (such as small micas or oxides) might form the dominant disorder. The results presented here could potentially provide a quantitative basis and prerequisite for more sophisticated numerical models of pressure solution (Ebner et al., 2009a; Koehn et al., 2007). We thus argue that the general idea of a general 'lithologic heterogeneity', which influences the stylolite morphology put forward by Railsback (1993), is correct but go further by demonstrating that the heterogeneities presented cause the characteristic roughness to develop and thus generate the stylolite. Consequently the current work offers strong

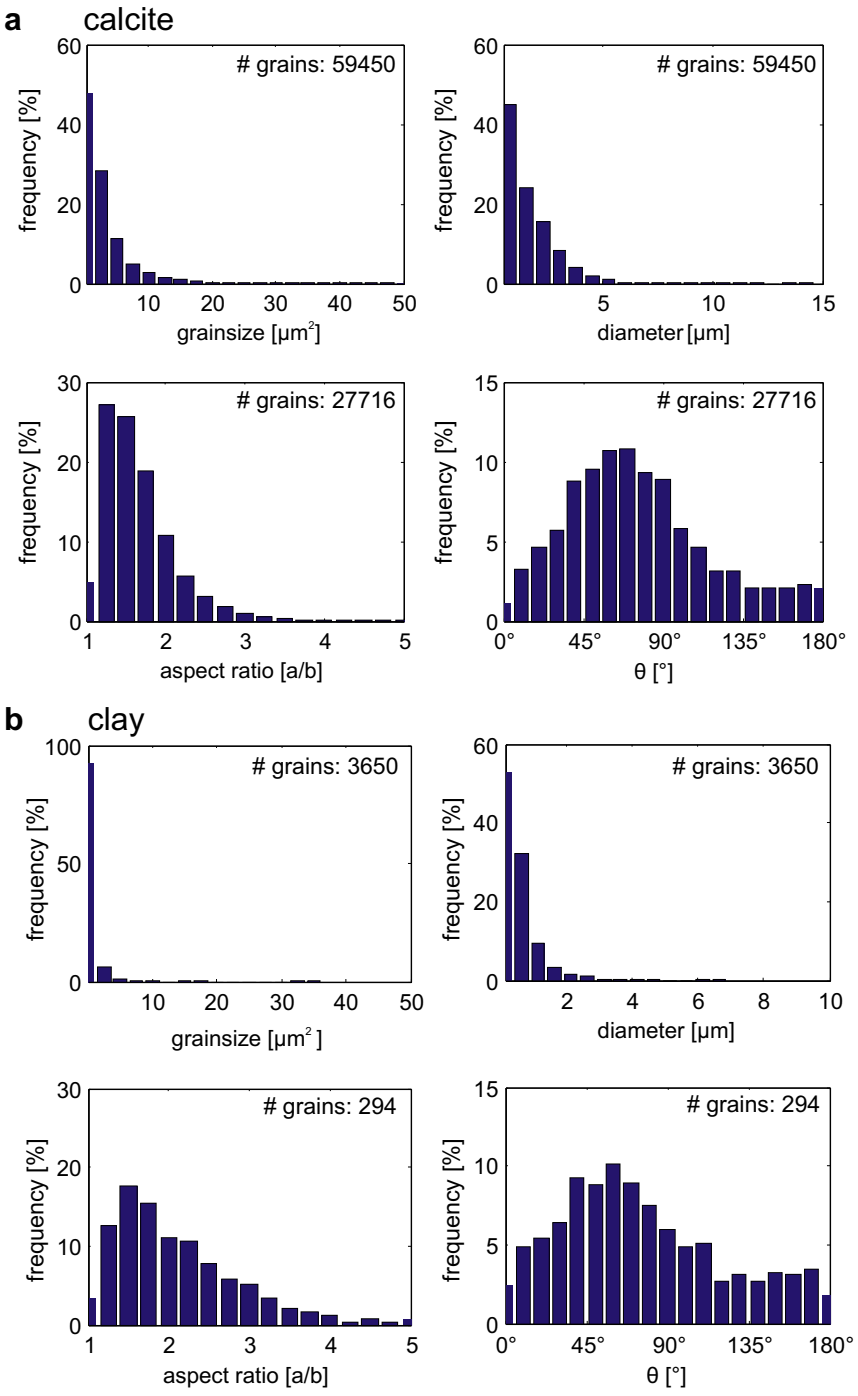

Fig. 8. Grain size and shape data set for the matrix around a mature stylolite interface (sample *Sa7b*) of a) calcite and b) clay particles (same representation as in Figs. 3 and 6). Note that the grain surface area of the clay particles is approximately one order of magnitude smaller than that of calcite (geometric mean of 0.12 µm^2 and 1.2 µm^2, respectively). The aspect ratio of the clay particles is significantly higher than that of the calcite grains but the SPO (θ) of both fractions is quite similar.

arguments that support a *heterogeneity concept* for the initiation of the stylolite roughness. Yet, this train of thought relies on the fact that the heterogeneities identified in the matrix surrounding the stylolite are similar to the heterogeneities found along the stylolite interface (i.e. assuming a passive enrichment during pressure solution). The clay minerals could as well have precipitated from a fluid that percolated along the stylolite. We think that this scenario can be excluded for the clays along initial stylolite interfaces which have not formed a continuous interface of residual material and for the quartz grains since the OC images (point EDX analysis not reported here) do not indicate a change in the composition of the heterogeneities. Such a change in composition cannot be precluded completely, especially for the more mature stylolite interfaces, without a detailed chemical analysis of the clay minerals.

4.2. Matrix modifications around stylolite interfaces

We observed changes in terms of grain size, SPO and LPO in the matrix adjacent to a stylolite. These changes complement the existing data of studies concentrating more on the porosity around stylolites (Baron and Parnell, 2007; Carrio-Schaffhauser et al., 1990; Harris, 2006; Raynaud and Carrio-Schaffhauser, 1992). In contrast

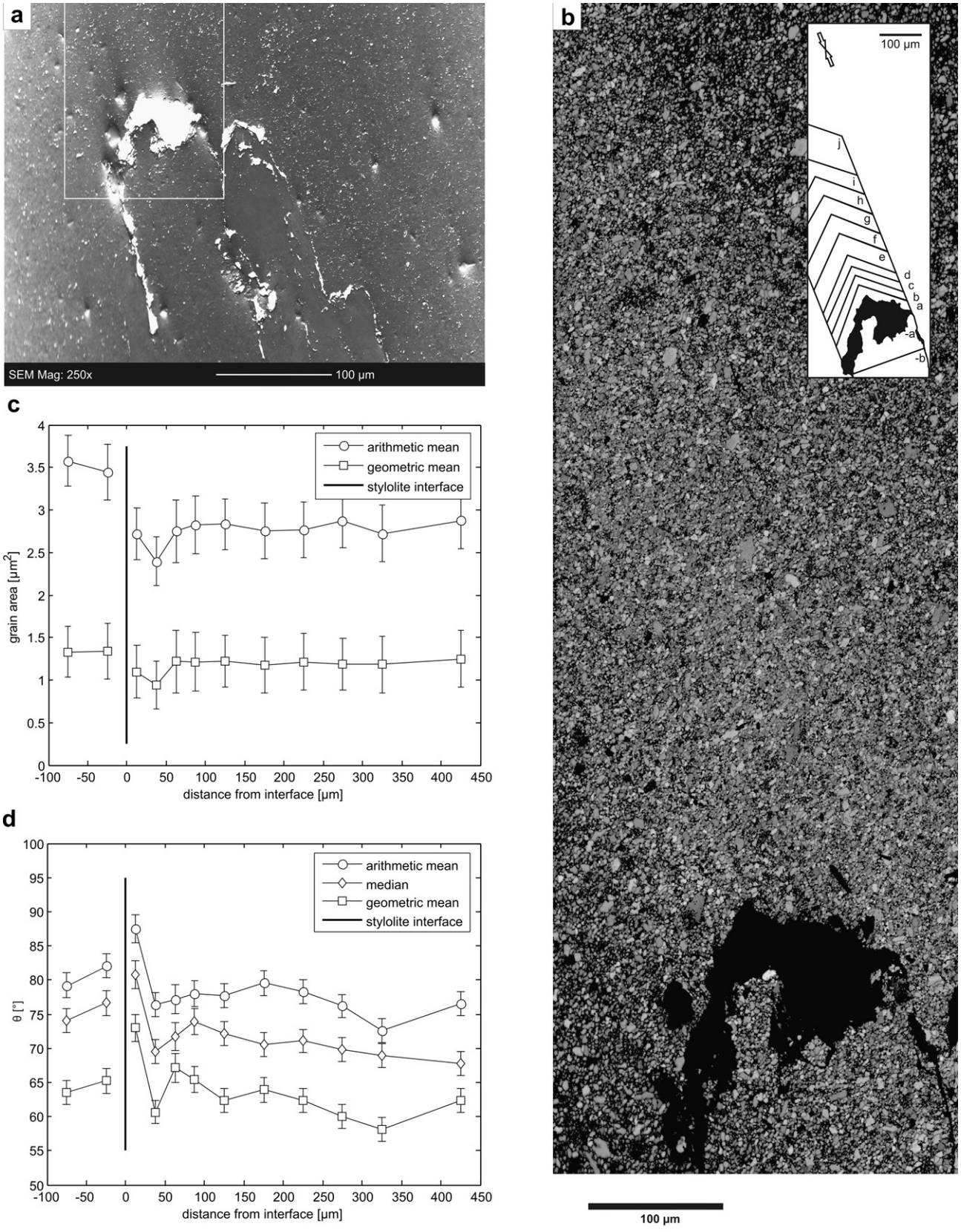

Fig. 9. Detailed investigation of the matrix as a function of the distance to the mature interface. a) OC image of the large asperity investigated along the tectonic stylolite of sample *Sa7b*. b) EBSD Band contrast of the surface area indicated in the white box of a) showing the outlines of individual grains and the stylolite peak in the lower part of the map. Inset shows the tectonic compaction direction (opposing arrows) and the position and outline of the investigated subsets labelled a–j (above the interface) and -a & -b (below the interface). c) Graph of the arithmetic and geometric mean surface area (μm^2) plotted as a function of the distance to the stylolite interface. d) The SPO i.e. θ is plotted as a function of the distance to the interface. The coefficient of variance is indicated by the error-bars shown in c–d.

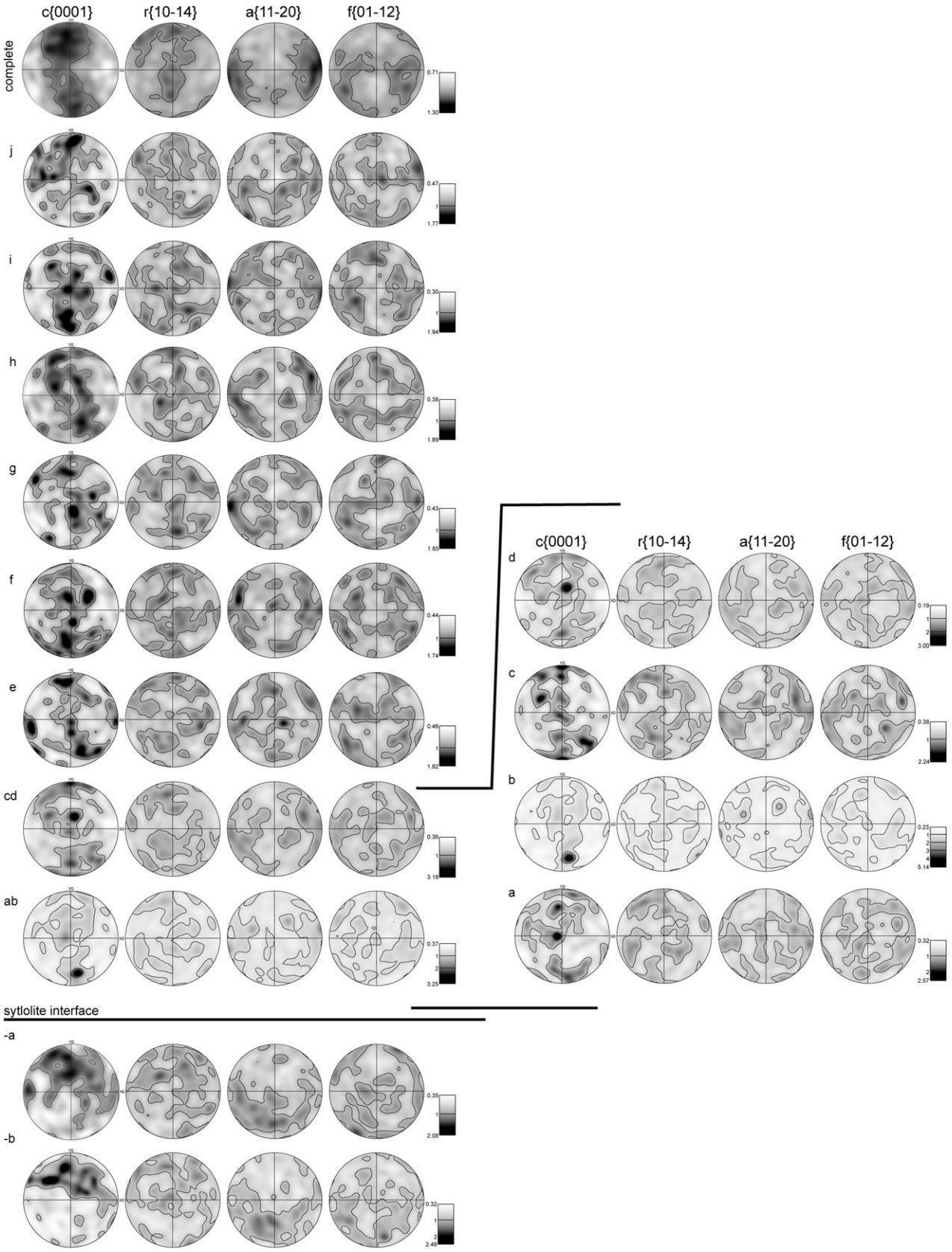

Fig. 10. Contoured pole figure plots of the LPO of calcite from the map in Fig. 9b (same representation as in Fig. 4). Top row shows the complete data set. The rows below represent the twelve subsets indicated in the inset of Fig. 9b (labelling refers to these subsets).

to the data reported by van Noort et al. (2009) and Mørk and Moen (2007), in our study we were unable to clearly attribute significant amounts of plastic deformation to the pressure solution along stylolite interfaces.

In our study we investigated a sample which allows distinguishing easily between the effect of soft sediment compaction structures and pressure solution imposed features as the investigated a tectonic stylolite trends normal to the sedimentary compaction direction. This high angle difference in the sedimentary and tectonic compaction direction allows us to decipher the effects of both events. Sedimentary compaction caused a strong SPO (Fig. 8a) and a weak LPO (Fig. 9) of the fine-grained calcite matrix surrounding the tectonic stylolite. Both SPO and LPO indicate a sedimentary compaction direction, which is roughly horizontal in Fig. 9b. Approaching the stylolite interface we found that in the matrix the (i) grain size (ii) SPO and (iii) LPO are modified.

The average grain size i.e. grain surface area of $\sim$3.0 μm^2 decreases some 15% (2.5 μm^2) in a region 25–75 μm away from the stylolite and finally increases to $\sim$3.0 μm^2 in the direct vicinity of the stylolite. Our results are quite similar to the data reported by Raynaud and Carrio-Schaffhauser (1992). But compared to the 'processes zones' of these authors, the region of reduced grain size we have identified is 1–2 orders of magnitude larger.

The sedimentary SPO (Fig. 7a), i.e. the average orientation of the long axis of calcite grains (θ), trending roughly N–S (due to E–W sedimentary compaction) is very well-defined. Evidence for N–S directed tectonic compaction that influences a broader zone around the stylolite would be indicated by a gradual decrease from high θ to low θ values. In fact we observed the opposite, the θ values slightly increase toward the interface. Only in the region of reduced grain size 25–75 μm away from the interface θ decreases some 5–10°. It is interesting to notice that the kurtosis, a measure for the asymmetry or 'peakedness' of a probability distribution, decreases towards the interface. This is an indication that the SPO gets obliterated toward the interface.

The weak sedimentary LPO is defined by c-axes being oriented in a great circle normal to the compaction direction (Fig. 10). In the vicinity of the stylolite (25–75 μm from the interface) this sedimentary LPO is overprinted by a relatively well-defined single maximum of c-axis parallel to the tectonic compaction direction. Numerical simulations (Bons and den Brok, 2000) showed that solution-precipitation creep can indeed play a role in the formation of an LPO. The model of Bons and den Brok (2000) is based on the observation that quartz has a directional anisotropy in the dissolution rate, *i.e.* c-axis exhibit the smallest amount of dissolution, and grains which have an orientation of 50° between the c-axis and the shortening direction have the highest amounts of dissolution (Becker, 1995; den Brok, 1996). This suggests a preferential dissolution of grains with their c-axis inclined 50° away from the compaction direction and in turn favours the development of an LPO. LPO measurements of uniaxial compaction experiments and theoretical considerations show c-axis maxima parallel to the compaction direction (Wenk, 1985; Wenk et al., 1987), which is in line with our findings (compare c-axis maxima in subsets a & b in Fig. 10). We are thus convinced that the LPO in the vicinity of the stylolite is a result of tectonic compaction.

Finally, we have to discuss the features in the matrix adjacent to the stylolite (<25 μm away from the interface). We observe that in this region the grain size increases by 15% and the SPO changes 15–25°, whereas the LPO shows a quasi random pattern. To explain these characteristics of the matrix two main scenarios seem possible. First, the stylolite interface (and probably its surrounding) remains fluid rich once the stresses have ceased. Thus static grain growth could occur in the stylolite vicinity due to high grain boundary mobility. Second, it is also conceivable that a fluid flow that post dates pressure solution could have deposited calcite cement in the intergranular pore space. Both scenarios could account for the grain size increase and the change in the SPO since more isometric grains would have an SPO, which will resemble a Gaussian distribution with a high variance and thus show a mean around 90° as observed in our data set. The obliteration of the LPO is harder to explain with this hypothesis since cements or static grain growth often show overgrowth, which has a similar crystallographic orientation as the host grain (Mørk and Moen, 2007). A possibility could be a process similar to Ostwald ripening (Morse and Casey, 1988) in the fluid filled vicinity of the stylolite interface. Ostwald ripening is a process which leads to preferential grain growth (i.e. large grains grow at the expense of small grains) to minimize the surface to volume ratio and thus the surface free energy. Such a surface minimization process could account for the grain size increase and, due to the preferential dissolution of the small grains, to a destruction of the SPO and possibly the LPO.

We hypothesize that mature interfaces form a 'mechanical layer', which is able to transmit stress and may induce intergranular pressure solution in a region around the stylolite, due to an undercutting mechanism (Lehner, 1995) or free face dissolution (Tada et al., 1987; Tada and Siever, 1989). Such a conceptual model would self- induce localized pressure solution and would explain the grain size reduction and a perturbation of the pre-existing sedimentary SPO and LPO, which we observed. On the scale of observation that was used in this work the stylolite does not represent a thin–film interface. Locally a thin film may exist, but on the scale of observation (micron-scale) the stylolite interface is complex, forms a stress-supported network and a large process zone.

5. Conclusion

In the present work we report a detailed qualitative and quantitative microstructural analysis based on EBSD/SEM and OC image analysis of stylolites in limestones. Our study sheds new light on the role of heterogeneities (in our case clay particles and detrital quartz grains) and reveals matrix adjustments around mature stylolite interfaces. The importance of heterogeneities for the morphological development was stressed in previous work (Andrews and Railsback, 1997; Railsback, 1993) and successfully applied in analytical (Renard et al., 2004; Schmittbuhl et al., 2004) and numerical models (Ebner et al., 2009a; Koehn et al., 2007). Data presented here provide direct observational evidence for a roughening of stylolites induced by heterogeneities on various scales. We conclude that indeed this multiscale quenched noise is responsible for the initiation of roughness along stylolites. In addition we demonstrate that around mature stylolite interfaces significant matrix modifications occur, which are not necessarily symmetric. By the investigation of tectonic stylolites with a bedding normal orientation we were able to discern the effects of sedimentary and tectonic compaction. This implies that localized pressure solution around stylolites imposes a halo with reduced grain size of 15–25% (depending on the use of mean or geometric mean grain-size), and a perturbed SPO and LPO.

Both findings are important to future research on pressure solution surfaces. First, it provides a quantitative basis for the development of more sophisticated numerical models and secondly it implies that localized pressure solution is not necessarily restricted to the actual interface.

Acknowledgements

M. Ebner and D. Koehn acknowledge support via DFG grant KO2114/5–1gs1 and F. Renard a support from ANR-09-JCJC-0011-01. M. Ahlbom is thanked for technical support during SEM/EBSD analysis.

References

Alvarez, W., Engelder, T., Geiser, P.A., 1978. Classification of solution cleavage in pelagic limestones. Geology 6 (5), 263–266.

Andrews, L.M., Railsback, L.B., 1997. Controls on stylolite development: morphologic, lithologic, and temporal evidence from bedding-parallel and transverse stylolites from the US Appalachians. Journal of Geology 105 (1), 59–73.

Angheluta, L., Jettestuen, E., Mathiesen, J., Renard, F., Jamtveit, B., 2008. Stress-driven phase transformation and the roughening of solid–solid interfaces. Physical Review Letters 100 (9), 096105.

Arnaud-Vanneau, A., Arnaud, H., 1990. Hauterivian to lower Aptian carbonate shelf sedimentation and sequence stratigraphy in the Jura and northern subalpine chains (Southeastern France and Swiss Jura). In: Tucker, M.E., Wilson, J.L., Crevello, P.D., Sarg, J.F., Read, J.F. (Eds.), Carbonate Platforms. Special Publications of the international Association of Sedimentologist, 9, 203–233.

Baron, M., Parnell, J., 2007. Relationships between stylolites and cementation in sandstone reservoirs: examples from the North Sea, U.K. and East Greenland. Sedimentary Geology 194 (1–2), 17–35.

Bathurst, R.G.C., 1987. Diagenetically enhanced bedding in argillaceous platform limestones – stratified cementation and selective compaction. Sedimentology 34 (5), 749–778.

Bayly, B., 1986. A mechanism for development of stylolites. Journal of Geology 94 (3), 431–435.

Becker, A., 1995. Quartz pressure solution: influence of crystallographic orientation. Journal of Structural Geology 17 (10), 1395–1397.

Bodou, P., 1976. Importance of the stylolitic joints in the compaction of limestones. Bulletin du Centre de Recherches Pau – SNPA 10 (2), 627–644.

Bonnetier, E., Misbah, C., Renard, F., Toussaint, R., Gratier, J.P., 2009. Does roughening of rock–fluid–rock interfaces emerge from a stress-induced instability? The European Physical Journal B – Condensed Matter and Complex Systems 67 (1), 121–131.

Bons, P.D., den Brok, B., 2000. Crystallographic preferred orientation development by dissolution–precipitation creep. Journal of Structural Geology 22 (11–12), 1713–1722.

den Brok, B., 1996. The effect of crystallographic orientation on pressure solution in quartzite. Journal of Structural Geology 18 (6), 859–860.

Brouste, A., Renard, F., Gratier, J.P., Schmittbuhl, J., 2007. Variety of stylolites' morphologies and statistical characterization of the amount of heterogeneities in the rock. Journal of Structural Geology 29 (3), 422–434.

Buxton, T.M., Sibley, D.F., 1981. Pressure solution features in a shallow buried limestone. Journal of Sedimentary Petrology 51 (1), 19–26.

Carrio-Schaffhauser, E., Raynaud, S., Latiere, H.J., Mazerolle, F., 1990. Propagation and localization of stylolites in limestones. In: Knipe, R.J., Rutter, E.H. (Eds.), Deformation Mechanics, Reology and Tectonics. Geological Society Special Publications, vol. 54, pp. 193–199.

Drummond, C.N., Sexton, D.N., 1998. Fractal structure of stylolites. Journal of Sedimentary Research 68 (1), 8–10.

Dunnington, H.V., 1954. Stylolite development post-dates rock induration. Journal of Sedimentary Petrology 24 (1), 27–49.

Ebner, M., Koehn, D., Toussaint, R., Renard, F., 2009a. The influence of rock heterogeneity on the scaling properties of simulated and natural stylolites. Journal of Structural Geology 31 (1), 72–82.

Ebner, M., Koehn, D., Toussaint, R., Renard, F., Schmittbuhl, J., 2009b. Stress sensitivity of stylolite morphology. Earth and Planetary Science Letters 277 (3–4), 394–398.

Ebner, M., Toussaint, R., Schmittbuhl, J., Koehn, D., Bons, P., 2010. Anisotropic scaling of tectonic stylolites: a fossilized signature of the stress field? Journal of Geophysical Research-Solid Earth 115, B06403. doi:10.1029/2009JB006649.

Etzold, A., Franz, M., Villinger, E., 1996. Schwäbische Alb – Stratigraphie, Tektonik, Vulkanismus, Karsthydrogeologie. Z. Geol. Wiss. 24 (1/2), 175–215.

Geyer, O.F., Gwinner, M.P., 1991. Geologie von Baden-Württemberg. Schweizerbart'sche Verlagsbuchhandlung, Stuttgart.

Gratier, J.P., Muquet, L., Hassani, R., Renard, F., 2005. Experimental microstylolites in quartz and modeled application to natural stylolitic structures. Journal of Structural Geology 27 (1), 89–100.

Guzzetta, G., 1984. Kinematics of stylolite formation and physics of the pressure-solution process. Tectonophysics 101 (3–4), 383–394.

Harris, N.B., 2006. Low-porosity haloes at stylolites in the feldspathic Upper Jurassic Ula sandstone, Norwegian North Sea: an integrated petrographic and chemical mass-balance approach. Journal of Sedimentary Research 76 (3), 444–459.

Heald, M.T., 1955. Stylolites in sandstones. Journal of Geology 63 (2), 101–114.

Heilbronner, R.P., 1992. The autocorrelation function: an image processing tool for fabric analysis. Tectonophysics 212 (3–4), 351–370.

Heilbronner, R., Keulen, N., 2006. Grain size and grain shape analysis of fault rocks. Tectonophysics 427 (1–4), 199–216.

Humphreys, F.J., 2001. Review – Grain and subgrain characterisation by electron backscatter diffraction. Journal of Materials Science 36 (16), 3833–3854.

Karcz, Z., Scholz, C.H., 2003. The fractal geometry of some stylolites from the Calcare Massiccio Formation, Italy. Journal of Structural Geology 25 (8), 1301–1316.

Kley, J., Voigt, T., 2008. Late Cretaceous intraplate thrusting in central Europe: effect of Africa–Iberia–Europe convergence, not Alpine collision. Geology 36 (11), 839–842.

Koehn, D., Renard, F., Toussaint, R., Passchier, C.W., 2007. Growth of stylolite teeth patterns depending on normal stress and finite compaction. Earth and Planetary Science Letters 257 (3–4), 582–595.

Lacombe, O., 2007. Comparison of paleostress magnitudes from calcite twins with contemporary stress magnitudes and frictional sliding criteria in the continental crust: mechanical implications. Journal of Structural Geology 29 (1), 86–99.

Lehner, F.K., 1995. A model for intergranular pressure solution in open systems. Tectonophysics 245 (3–4), 153–170.

Marshak, S., Engelder, T., 1985. Development of cleavage in limestones of a fold-thrust belt in eastern New York. Journal of Structural Geology 7 (3–4), 345–359.

Mingard, K.P., Roebuck, B., Bennett, E.G., Thomas, M., Wynne, B.P., Palmiere, E.J., 2007. Grain size measurement by EBSD in complex hot deformed metal alloy microstructures. Journal of Microscopy 227 (3), 298–308.

Morse, J.W., Casey, W.H., 1988. Ostwald processes and mineral paragenesis in sediments. American Journal of Science 288 (6), 537–560.

Moss, S., Tucker, M.E., 1995. Diagenesis of Barremian–Aptian platform carbonates (the Urgonian limestone formation of SE France): near-surface and shallow-burial diagenesis. Sedimentology 42 (6), 853–874.

Mørk, M.B.E., Moen, K., 2007. Compaction microstructures in quartz grains and quartz cement in deeply buried reservoir sandstones using combined petrography and EBSD analysis. Journal of Structural Geology 29 (11), 1843–1854.

van Noort, R., Spiers, C.J., Pennock, G.M., 2008. Compaction of granular quartz under hydrothermal conditions: controlling mechanisms and grain boundary processes. Journal of Geophysical Research – Solid Earth 113, B12206. doi:10.1029/2008JB005815.

Panozzo, R.H., 1983. Two-dimensional analysis of shape–fabric using projections of digitized lines in a plane. Tectonophysics 95 (3–4), 279–294.

Park, W.C., Schot, E.H., 1968. Stylolites: their nature and origin. Journal of Sedimentary Petrology 38 (1), 175–191.

Passchier, C.W., Trouw, R.A.J., 2005. Microtectonics. Springer, Berlin.

Petit, J.P., Mattauer, M., 1995. Palaeostress superimposition deduced from mesoscale structures in limestone: the Matelles exposure, Languedoc, France. Journal of Structural Geology 17 (2), 245–256.

Prior, D.J., Trimby, P.W., Weber, U.D., Dingley, D.J., 1996. Orientation contrast imaging of microstructures in rocks using forescatter detectors in the scanning electron microscope. Mineralogical Magazine 60 (6), 859–869.

Prior, D.J., Boyle, A.P., Brenker, F., Cheadle, M.C., Day, A., Lopez, G., Peruzzi, L., Potts, G., Reddy, S., Spiess, R., Timms, N.E., Trimby, P., Wheeler, J., Zetterstrom, L., 1999. The application of electron backscatter diffraction and orientation contrast imaging in the SEM to textural problems in rocks. American Mineralogist 84 (6), 1741–1759.

Railsback, L.B., 1993. Lithologic controls on morphology of pressure-dissolution surfaces (stylolites and dissolution seams) in Paleozoic carbonate rocks from the mideastern United States. Journal of Sedimentary Research 63 (3), 513–522.

Raynaud, S., Carrio-Schaffhauser, E., 1992. Rock matrix structures in a zone influenced by a stylolite. Journal of Structural Geology 14 (8–9), 973–980.

Renard, F., Schmittbuhl, J., Gratier, J.P., Meakin, P., Merino, E., 2004. Three-dimensional roughness of stylolites in limestones. Journal of Geophysical Research–Solid Earth 109, B03209. doi:10.1029/2003JB002555.

Rispoli, R., 1981. Stress-fields about strike-slip faults inferred from stylolites and tension gashes. Tectonophysics 75 (3–4), T29–T36.

Schmittbuhl, J., Renard, F., Gratier, J.P., Toussaint, R., 2004. Roughness of stylolites: implications of 3D high resolution topography measurements. Physical Review Letters 93 (23).

Stockdale, P.B., 1922. Stylolites: their nature and origin. Indiana University Studies 9, 1–97.

Tada, R., Maliva, R., Siever, R., 1987. A new mechanism for pressure solution in porous quartzose sandstone. Geochimica et Cosmochimica Acta 51 (9), 2295–2301.

Tada, R., Siever, R., 1989. Pressure solution during diagenesis. Annual Review of Earth and Planetary Sciences 17, 89–118.

Wenk, H.R., 1985. Preferred Orientation in Deformed Metals and Rocks: An Introduction to Modern Texture Analysis. Academic Press, Orlando (FL).

Wenk, H.R., Takeshita, T., Bechler, E., Erskine, B.G., Matthies, S., 1987. Pure shear and simple shear calcite textures. Comparison of experimental, theoretical and natural data. Journal of Structural Geology 9 (5–6), 731–745.